Journal of Materials Chemistry A

Accepted Manuscript

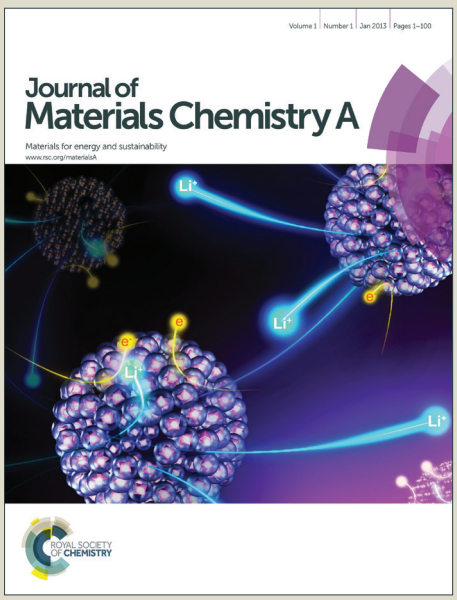

ROYAL SOCIETY OF CHEMISTRY

www.rsc.org/materialsA

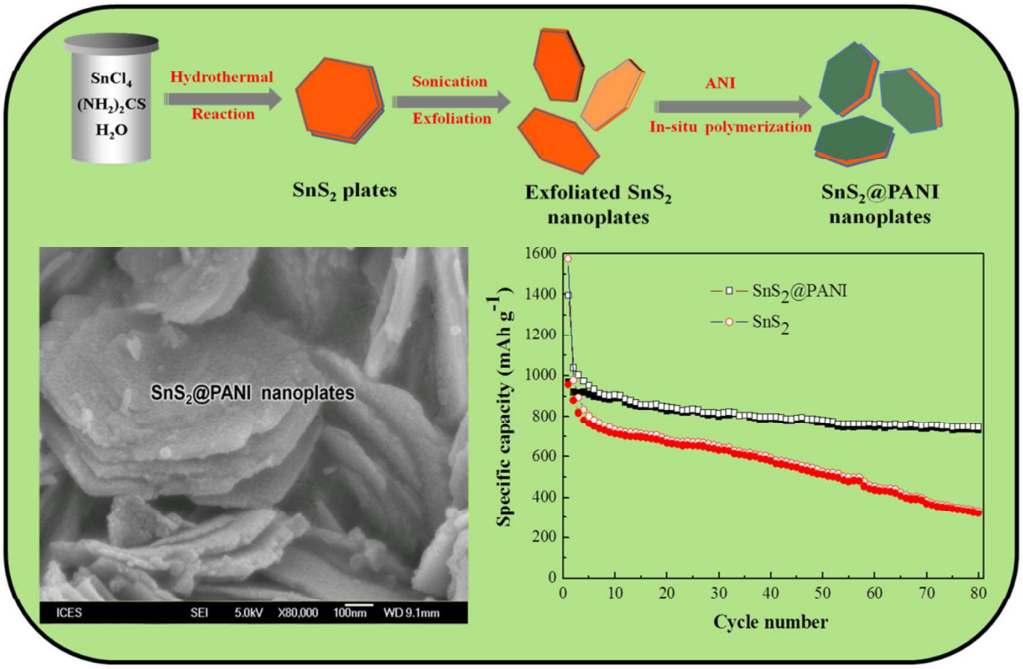

Cite this: DOI: 10.1039/c0xx00000x

www.rsc.org/xxxxxx

ARTICLE TYPE

Two-dimensional SnS_2@PANI nanoplates with high capacity and excellent stability for lithium-ion batteries

Gang Wang[a*], Jun Peng[a], Lili Zhang[b], Jun Zhang[c], Bin Dai[a*], Mingyuan Zhu[a], Lili Xia[d], Feng Yu[a*]

Received (in XXX, XXX) Xth XXXXXXXXX 20XX, Accepted Xth XXXXXXXXX 20XX
DOI: 10.1039/b000000x

Nanostructured electrode materials have been studied extensively with the aim of enhancing lithium ion and electron transport and lowering the stress caused by their volume changes during the charge/discharge processes of electrodes in lithium-ion batteries. In this work, a novel two-dimensional nanocomposite, polyaniline-coated SnS_2 (SnS_2@PANI) nanoplates, has been prepared by in situ oxidative polymerization of aniline on the surface of ultrasonic exfoliated SnS_2 nanoplates. The SnS_2@PANI nanoplates present a lamellar sandwich nanostructure, which it can provide a good conductive network between neighboring nanoplates, shorten the path for ions transport in the active material, and alleviate the expansion and contraction of the electrode material during the charge/discharge processes, leading to an improved electrochemical performance. As an anode material for lithium-ion batteries, SnS_2@PANI nanoplates have a high initial reversible capacity (968.7 mAh g^{-1}), excellent cyclability (730.8 mAh g^{-1} after 80 cycles, corresponding to 75.4% of the initial reversible capacity) and extraordinary rate capability (356.1 mAh g^{-1} at the rate of 5000 mA g^{-1}). This study not only provides a simple and efficient synthesis strategy for various inorganic–organic composites obtained by exfoliation of layered inorganic materials, but also helps in designing novel and high performance electrode materials.

[a] *School of Chemistry and Chemical Engineering, Key Laboratory for Green Processing of Chemical Engineering of Xinjiang Bingtuan, Shihezi University, Shihezi, P.R. China. E-mail:gwangshzu@163.com (G. Wang), daibin_bce@shzu.edu.cn (B. Dai) and yufeng05@mail.ipc.ac.cn (F. Yu).*
[b] *Institute of Chemical and Engineering Sciences, Agency for Science, Technology and Research, Jurong Island, Singapore*
[c] *School of Material Science and Engineering, University of Jinan, Jinan, P.R. China*
[d] *Radiation and Hazardous Wastes Supervision Center of Shiyan, Shiyan, P.R. China*

Cite this: DOI: 10.1039/c0xx00000x

www.rsc.org/xxxxxx

ARTICLE TYPE

1. Introduction

Rechargeable Li-ion batteries (LIBs) are now considered as the most important power sources for electric vehicles (EVs) and hybrid electronic vehicles (HEVs). In order to meet the increasing requirements for EVs and HEVs applications, lithium-ion batteries with larger energy density, higher power density, and longer cycle life are highly desirable.[1,2] However, the relatively low storage capacity (372mAh g^{-1}) of commercially used graphite carbon still restricts its application in LIBs with high energy and power density. Therefore, much research interests have been prompted to focus on new anode materials.

In terms of meeting the requirements of new generation electrode materials for LIBs, SnS_2 have been suggested as one of most potential substitute for the state-of-the-art graphite anode to increase the battery capacity. SnS_2 has a layered CdI_2-type structure, composed of tin atoms sandwiched between two layers of hexagonally disposed close packed sulfur atoms.[3,4] It is believed the spacious configuration is more tolerant of cycling-induced volume excursions and enhances the accessibility of the Li host.[5,6] Unfortunately, the capacity fading of SnS_2 electrode materials still exists due to the large volume changes and poor electrical conductivity during the electrochemical alloy formation. A variety of appealing strategies have been utilized to solve these intractable problems, including the use of carbon-based nanocomposites[4,7-18] and unique SnS_2 nano/microstructures of 3-dimensional (3D) flower-like SnS_2,[19,20] 3D hierarchical SnS_2 microspheres,[21] 2D layered SnS_2 nanoplates[3,22] and nanosheets.[23,24] In particular, the combination of SnS_2 with graphene has become favourable due to their unique properties such as larger surface area, greater accessibility to electrolyte, and high-rate transportation of electrons throughout the electrode matrix.[10,13] However, the complicated synthesis procedure and the use of toxic reagent (such as hydrazine or sodium borohydride) for high quality graphene might limit the practical applications of the composites. Compared to those well-reported SnS_2-graphene nanocomposites, there has been barely report on combining SnS_2 with conducting polymers for LIBs. Polyaniline (PANI) is considered as one of the most promising conducting polymers because of its easy synthesis, low cost, good electron conductivity and environmental stability.[25,26] These characteristics make it a ideal buffering matrix to accommodate active materials for electrochemical energy storage purposes.[27-29] Thus, it is necessary to explore this novel protocols for SnS_2 to enhance its electrochemical performance for LIBs.

Herein, we report for the first time a facile approach towards two-dimensional (2D) polyaniline-coated SnS_2 (SnS_2@PANI) nanoplates by in situ oxidative polymerization of aniline on the surface of ultrasonic exfoliated SnS_2 nanoplates. As illustrated in Scheme 1, the overall synthetic procedure of SnS_2@PANI nanoplates involves three steps. SnS_2 plates are firstly synthesized by a facile hydrothermal method. The obtained SnS_2 plates were exfoliated by ultrasonic treatment and then coated by in situ oxidative polymerization of aniline. As a result, a novel 2D sandwich nanostructure composed of SnS_2@PANI nanoplates was obtained. What's more, the SnS_2@PANI nanoplates displays superior LIBs performance with large reversible capacity, high coulombic efficiency, excellent cyclic performance, and good rate capability, which could be employed as excellent anode materials for high-performance LIBs.

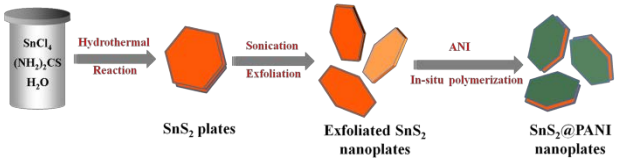

Scheme 1 Schematic illustration for the formation of SnS2@PANI nanoplates

2. Experimental Section

2.1 Synthesis of SnS_2 plates: In a typical experiment, amounts of $SnCl_4$ and thiourea in the stoichiometric ratio of 1:2 were dissolved in 50 mL deionized water and stirred until totally dissolved. The volume of the reaction solution was set to 60 mL by adding deionized water. Unless otherwise mentioned, no other reagents were added into the reaction solution. The reaction solution was then transferred into a 100 mL Teflon-lined stainless steel autoclave and heated slowly to 180℃ and kept for 12h. Afterward, the autoclave was cooled to room temperature naturally and the yellow products were isolated by centrifugation, rinsed several times with distilled water, and then vacuum-dried at 60℃ to obtain the pristine SnS_2.

2.2 Synthesis of SnS_2@PANI Nanoplates: SnS_2 nanosheets were first obtained by ultrasonic exfoliation method. The pristine SnS_2 was dispersed in ethanol and was sonicated for 4h, and then placed in an ice bath and was constantly stirred with a magnetic stirrer. Aniline monomer was diluted with ethanol and then was added slowly into the above mixture under stirring. Subsequently, ammonium persulfate and $LiClO_4$ was slowly added into the solution to start the oxidation process. The reaction vessel was kept in the ice bath with constant stirring for 24h. The product was then washed repeatedly by deionized water and ethanol to remove the residual reactant. The final product was dried at 120℃ for 24h.

2.3 Physical characterization of the synthesized samples: The crystalline structures of pristine SnS_2 and as-obtained SnS_2@PANI nanoplates were studied by a X-ray diffractometer (XRD, Bruker D8 focus), with Cu Kα radiation (λ=1.5406Å) at 40kV, 40mA, step size of 0.02°, and a count time of 0.6s per step between 2θ=10° and 90°. The scanning electron microscopy (SEM) images were obtained using a scanning electron microscope (JEOL JSM-7600F) operated at 10kV. Transmission electron microscopy (TEM) and high-resolution TEM (HRTEM) images patterns were taken by a field emission transmission

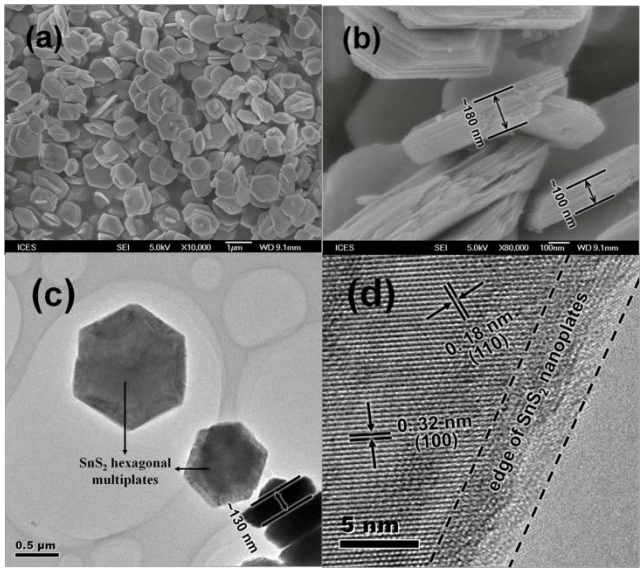

Fig. 1 (a, b) SEM images of the pristine SnS_2 plates at different magnifications. (c) TEM images of the pristine SnS_2 plates. (d) A HRTEM image of the edge of SnS_2 plates.

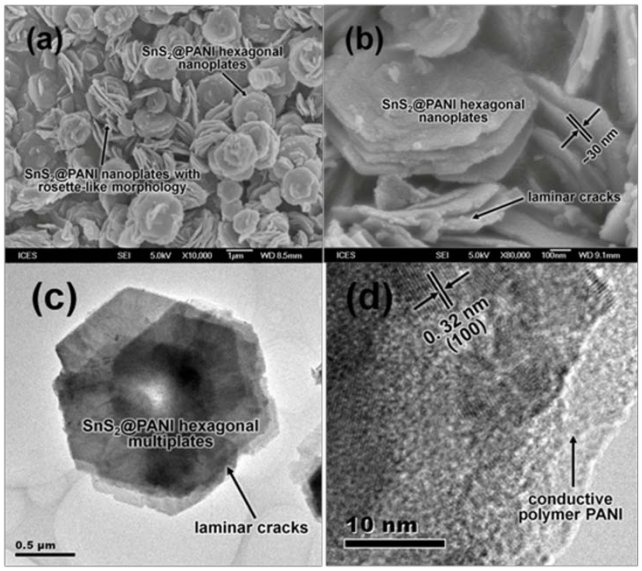

Fig. 2 (a, b) SEM images of the as-synthesized SnS_2@PANI nanoplates at different magnifications. (c) TEM image of the as-synthesized SnS_2@PANI nanoplates. (d) HRTEM images of SnS_2@PANI nanoplates.

electron microscopy (Philips Tecnai-F20). SEM and TEM were used for observing the morphology of the prepared powders. HRTEM were applied to detect the crystal lattice of SnS_2. Thermogravimetry analysis (TGA) was carried out on a simultaneous thermal analyzer (NETZSCH STA 449 F3) in an air atmosphere from room temperature to 700℃ at a rate of 10℃ min^{-1}.

2.4 Electrochemical measurement: For fabrication of the working electrodes, the pristine SnS_2 and as-obtained SnS_2@PANI nanocomposites were mixed respectively with acetylene black and polyvinylidene fluoride (PVDF) in a weight ratio of 80:10:10 in N-methyl-2 pyrrolidinone (NMP). The obtained slurry was coated onto Cu foil and dried at 120℃ for 12h. The dried tape was then punched into round plates with diameter of 12.0 mm as the cathode electrodes. Finally, the prepared cathodes and Celgard2400 separator (diameter of 16.0mm) were placed into an argon atmosphere filled glove box (H_2O and O_2<1ppm) and assembled into a coin cell (CR2032) with a lithium anode, electrolyte of 1M $LiPF_6$ in EC-DEC-EMC (1:1:1 vol.%) and the other components of the coin-type cell. The cells were examined with capacity retention studies performed at various rates between 0.01V-3.0V (vs Li^+/Li) via Maccor Series 4200 standard battery test system. The specific capacity of SnS_2@PANi nanocomposites was calculated based on the total mass of the SnS_2@PANi nanocomposites. Cyclic voltammograms(CVs) and electrochemical impedance spectra (EIS) were carried out using an Autolab PGSTAT30 electrochemical workstation at room temperature.

3. Results and discussion

3.1 Morphological characterization

Fig. 1 shows SEM and TEM images of the pristine SnS_2 plates prepared by hydrothermal method. The SEM image (Fig. 1a) illustrates that the pristine SnS_2 has hexagonal plates morphology and shows good uniformity of the morphology. The high magnification SEM image (Fig. 1b) shows the pristine SnS_2 plates with an average thickness of ca. 150nm are composed of many SnS_2 monolayers. It is believed that SnS_2 monolayers can be stacked along the [001] direction by van der Waals interactions.[3] The TEM image (Fig. 1c) further confirms that the pristine SnS_2 are 2D hexagonal plates with a lateral size of ca. 700nm. A more revealing feature of the crystallographic structures of the pristine SnS_2 plates comes from HRTEM analysis (Fig. 1d). The lattice spacings of 0.18 and 0.32 nm correspond to the (110) plane and (100) plane, respectively, of SnS_2.

Fig. 2 shows SEM and TEM images of the as-synthesized SnS_2@PANI nanoplates. The SEM image (Fig. 2a, b) illustrates that the SnS_2@PANI nanoplates still retained the hexagonal plate-like morphology with a rough surface. It is also evident that the SnS_2@PANI nanoplates are more thinner than the pristine SnS_2 plates. As is well known, the connection between the S-Sn-S layers is weak van der Waals interactions, making it easy to be separated. In this study, SnS_2@PANI nanoplates with an average thickness of ca. 40nm are obtained by employing ultrasonic exfoliation method. Due to edge-to-surface interactions of the nanoplates,[20] some thin SnS_2@PANI nanoplates aggregated into loose rosette-like structures, which was not observed in pristine SnS_2 samples. The TEM image (Fig. 2c) clearly showed the exfoliated status of the as-synthesized SnS_2@PANI nanoplate and further confirms that the SnS_2@PANI nanoplate still retained the hexagonal plate-like morphology. The HR-TEM image in Fig. 2d revealed that the lattice fringe of SnS_2 in SnS_2@PANI nanoplate is not clear, because amorphous PANI coats the outer surface of SnS_2 nanoplate.

The formation of SnS_2@PANI nanoplates is attributed to the presence of SnS_2 nanoplates, which it acts as a template to supply a large number of active sites for the nucleation of polyaniline. During the polymerization, the anilinium cations are easy to be absorbed onto the surface of electronegative SnS_2, and polyaniline synthesized is also firmly bounded on the surface of SnS_2 nanoplates due to an electrostatic attraction between the surface of electronegative SnS_2 and doped polyaniline with

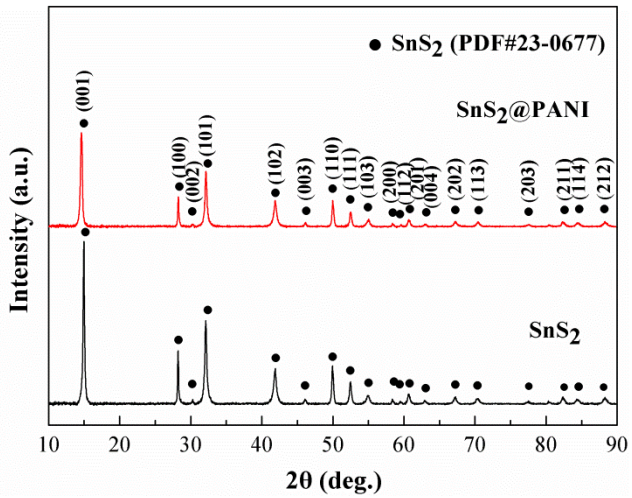

Fig. 3 XRD patterns of pristine SnS_2 and the as-synthesized SnS_2@PANI nanoplates.

positive charges on the backbone,[30] leading to the formation of two-dimensional sandwich-like SnS_2@PANI nanoplates. It is believed that the lamellar sandwich structure facilitated more lithium ions insertion and improved their cycling stability.

3.2 Structural characterization

Fig. 3 shows the XRD patterns of pristine SnS_2 and the as-synthesized SnS_2@PANI nanoplates. The XRD pattern of SnS_2@PANI nanoplates is similar with that of pristine SnS_2, in which all of the diffraction peaks can be assigned to the hexagonal SnS_2 (JCPDS Card no. 23−0677). However, SnS_2 in SnS_2@PANI nanoplates shows an obviously decreased relative intensity of (001) peak to other peaks compared with pristine SnS_2, which could be attributed to the ultrasonic exfoliation of pristine SnS_2 plates. According to the Scherrer equation ($D=K\lambda/\beta\cos\theta$), the average c-stacking height, calculated from the (0 0 1) reflection of SnS_2, was 143.3 nm for pristine SnS_2 and 49.1 nm for SnS_2@PANI nanoplates, which are consistent with the observed SEM results.

3.3 TG analysis

The content of PANI in the SnS_2@PANI nanoplates was determined by TG analysis in an air atmosphere at a heating rate of 10℃ min^{-1}, as shown in Fig. 4. The data presented in Fig. 4a suggests the TG curve of the as-synthesized SnS_2@PANI nanoplates shows a three-step mass-loss process. A small weight loss of 3.4% from room temperature to 200℃ could be attributed to the removal of physically adsorbed water and the loss of residual aniline oligomers near the crystallite edges.[28] The second weight loss between 200℃ and 450℃ could be ascribed to combustion of PANI in the hybrid nanoplates.[30] A further weight loss observed from 450℃ to 700℃ is attributed to the oxidation of SnS_2 into SnO_2,[31] and thus the final annealed product was well-indexed to tetragonal phase of SnO_2 [JCPDS 41-1445] (Fig. 4b). The total weight loss suffered by the nanoplates up to a temperature of 700 ℃ was 37.3%. Accordingly, the weight fraction of PANI in SnS_2@PANI nanoplates was calaclated to be ca. 20.5%. The high aspect ratio of the polymer component contributes to the advantage of constructing the conducting network.

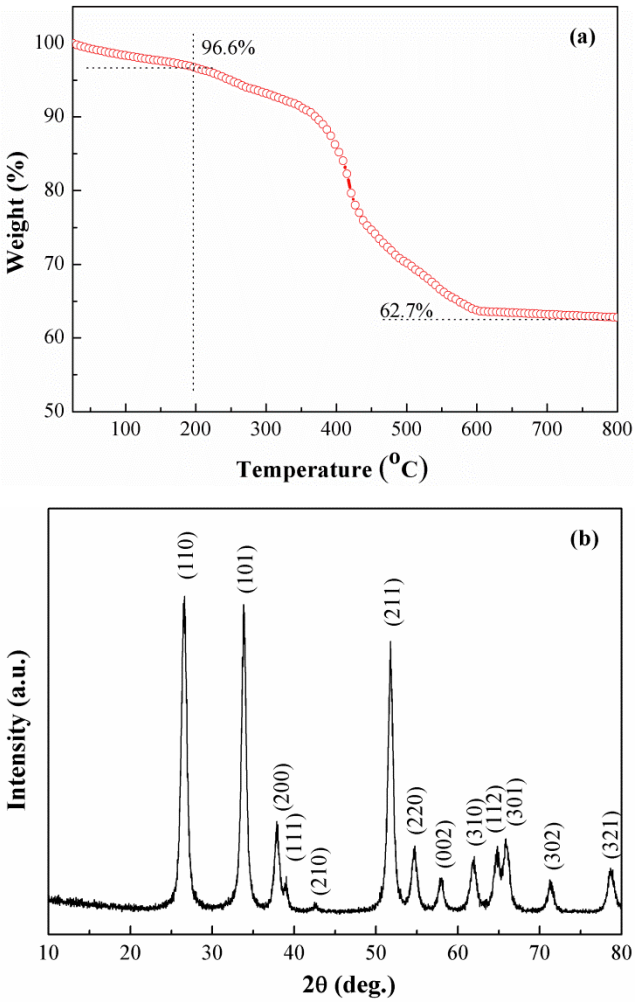

Fig. 4 (a) TGA curves of the as-synthesized SnS_2@PANI nanoplates and (b) XRD patterns of the residue of SnS_2@PANI nanoplates after thermogravimetric analysis.

3.4 Electrochemical performance

The electrochemical properties of the as-synthesized SnS_2@PANI nanoplates as Li-ion battery anode were investigated using a two-electrode cell with lithium metal as the counter electrode. Fig. 5 compare the cyclic voltammograms (CVs) of pristine SnS_2 and the as-synthesized SnS_2@PANI electrodes cycled between 0.01 and 3.0 V (vs Li^+/Li) at a scan rate of 0.1 mV s^{-1}. For the as-synthesized SnS_2@PANI electrode, as shown in Fig. 5b, the reduction peak at 1.76 V (vs Li^+/Li) in the first cathodic scan, which was not yet observed during the subsequent cycles, could be attributed to the lithium intercalation of the SnS_2 layers without phase decomposition(Eqs. (1)).[18,23,32] The reduction peaks at 1.52, 1.16 and 0.92 V (vs Li^+/Li) in the first cathodic sweep corresponded to the decomposition of the SnS_2 into metallic tin and the formation of Li_2S (Eqs. (2)), that may occurred in three steps as suggested by Kim et al.,[23] as well as the formation of solid electrolyte interface (SEI).[4,10] The peak at blew 0.30 V (vs Li^+/Li) in the first cathodic scan represented the reversible formation Li_xSn alloy (Eqs. (3)). The oxidation peak at 0.6 V (vs Li^+/Li) in the first anodic scan were known to represent the delithiation reaction of Li_xSn alloy (Eq. (3)), while another oxidation peak at 1.87 V (vs Li^+/Li) possibly originated

Cite this: DOI: 10.1039/c0xx00000x

www.rsc.org/xxxxxx

ARTICLE TYPE

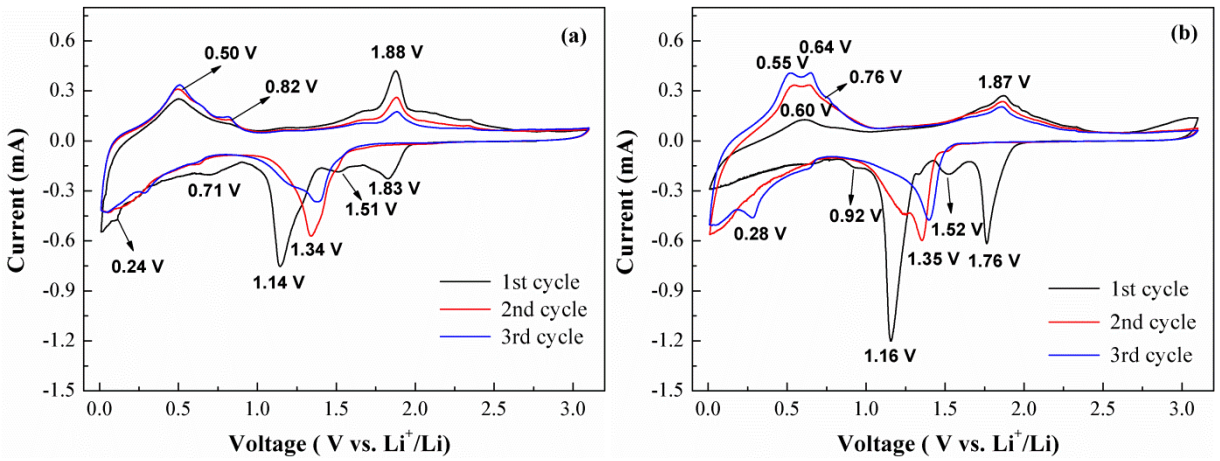

Fig. 5 Cyclic voltammograms of (a) SnS_2 and (b) SnS_2@PANI electrodes cycled between 0.01 and 3.0 V (vs Li^+/Li) at a scan rate of 0.1 mV s^{-1}.

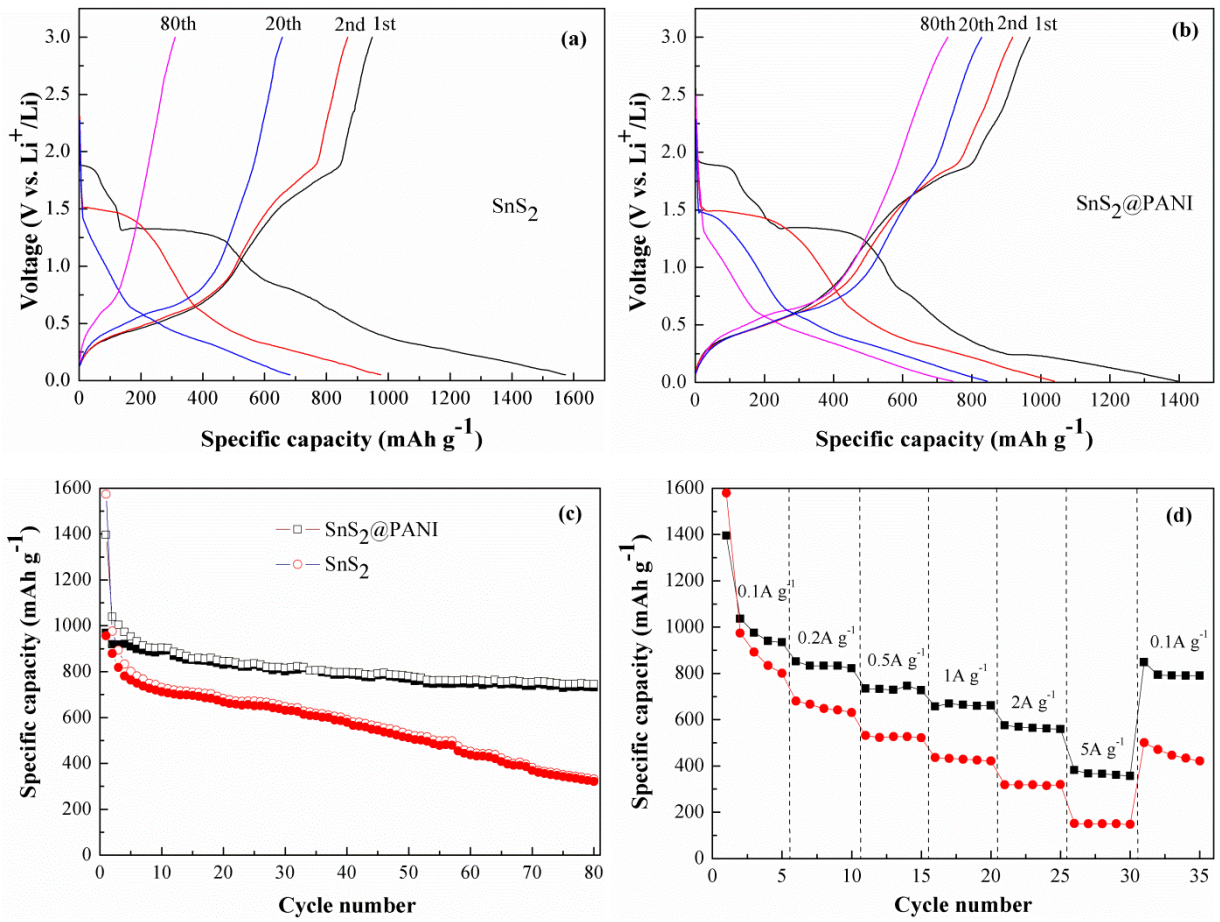

Fig. 6 Galvanostatic discharge–charge curves of (a) SnS_2 and (b) SnS_2@PANI cycled at the 1st, 2nd, 20th, and 80th between 0.01 and 3 V (vs Li^+/Li) at a current density of 100 mA g^{-1};(c) Cycling stability of SnS_2 and SnS_2@PANI at a current density of 100 mAg^{-1}; (d) Rate performance of SnS_2 and SnS_2@PANI at various current densities between 100 and 5000 mA g^{-1}.

from the oxygenation of Sn nanoparticles at higher potential in the charged state (Eq. (4)),[11,33,34] which also contributes to the rather high capacity and also the small first irreversible loss. The CV curves of pristine SnS_2 were displayed in Fig. 5a, which were

rather similar with those of the SnS_2@PANI nanoplates electrode, indicating similar electrochemical reaction pathway occurred during the intercalation/de-intercalation of lithium ions. The comprehensive mechanisms can be described by the electrochemical conversion reaction:[20,23]

$$SnS_2 + xLi^+ + xe^- \rightarrow Li_xSnS_2 \quad (1)$$

$$Li_xSnS_2 + (4-x)Li^+ + (4-x)e^- \rightarrow Sn + 2Li_2S \quad (2)$$

$$Sn + 4.4Li^+ + 4.4e^- \leftrightarrow Li_{4.4}Sn \quad (3)$$

$$SnS_2 + 4Li^+ + 4e^- \leftrightarrow Sn + 2Li_2S \quad (4)$$

In the second and subsequent cycles, the oxidation peak at 1.87 V (vs Li^+/Li) still appears, indicating the decomposition of Li_2S and recovery of SnS_2 is partially reversible based on Eqs. (4) at a high charge voltage. However, the current density and the integrated area of the SnS_2@PANI nanoplates are larger than those of the pristine SnS_2, and the peak at 1.87 V (vs Li^+/Li) for the second or third cycle of the SnS_2@PANI nanoplates which can be indexed to the reversible reaction to SnS_2, are more obvious and intensive than those of the pristine SnS_2, suggesting that the well-connected 2D networked structures of the SnS_2@PANI nanoplates lead to sufficient oxidation reaction process during the anodic cycling.

Lithium-storage properties of the pristine SnS_2 and SnS_2@PANI nanoplates were investigated by galvanostatic discharge–charge measurements. Fig. 6a and b compares the 1st, 2nd, 20th and 80th discharge and charge profiles of the pristine SnS_2 and SnS_2@PANI nanoplates electrodes at a current density of 100 mA g^{-1} in the voltage window of 0.01–3 V (vs Li^+/Li). It was found that the discharge/charge voltage profiles for the pristine SnS_2 and SnS_2@PANI nanoplates are very similar and are consistent with their corresponding CV plots. The initial discharge and charge capacities are 1573.5 and 947.8 mAh g^{-1} for the pristine SnS_2 electrode, and 1395.8 and 968.7 mAh g^{-1} for the SnS_2@PANI nanoplates electrode respectively. The initial discharge capacity for the two electrode materials are much higher than the maximum theoretical value of 1232 mAh g^{-1} based on Eq. (3) and Eq. (4).[14] This phenomenon has also been reported for SnO_2 and SnO and was ascribed to the formation of a polymeric gel-like film on the particle electrode surface.[35,36] The initial capacity loss may result from the incomplete conversion reaction and the irreversible loss of Li ions due to the formation of a SEI layer as discussed above.[9,23] It is interesting to note that the initial coulombic efficiency for the SnS_2@PANI nanoplates electrode is 69.4%, which was higher than that of carbon-coated SnS_2(41%),[7] SnS_2-graphene(69%),[14] SnS_2/G-As(37%),[11] few-layer SnS_2/graphene(42.4%)[9] and SnS_2@MWCNTs (37.2%),[5] indicating high charge/discharge reversibility of the SnS_2@PANI nanoplates electrode. Reasons for this phenomenon are still unclear, but it might be linked to PANI coating layers. We suggest that the presence of the PANI layers reduces the exposed surface edges to the electrolyte due to the shielding effect and results in a more conductive and thinner SEI film, which is favorable to the reversible intercalation and deintercalation of Li ions.[37] From the second cycle, the SnS_2@PANI nanoplates electrode presents much better electrochemical lithium storage performance than the pristine SnS_2 electrode. After twenty discharge/charge cycles, it exhibits a high reversible capacity of 828.8 mAh g^{-1}. The coulombic efficiency rapidly rises from 69.4% in the first cycle to 98.1% in the 20th one and then remains above 98% in the 80th cycle (Fig. 6b). In contrast, the reversible capacity of the pristine SnS_2 electrode rapidly drops to 657.3 mAh g^{-1} with a low coulombic efficiency of 96.3% after the 20th cycle and then gradually decreases to 94.1% for the 80th cycle (Fig. 6a). More importantly, the SnS_2@PANI nanoplates exhibit much better cycling performance than the pristine SnS_2 (Fig. 6c). It can be seen that the reversible capacity of the pristine SnS_2 decreases from 947.8 to only 311.2 mAh g^{-1} up to 80 cycles with only capacity retention rate of 32.8%. In contrast, the reversible capacity of the SnS_2@PANI nanoplates slightly decreases with cycling and reaches 730.8 mAh g^{-1} after 80 cycles, showing high capacity retention of 75.4%, which were positive in comparison with the previous results for tin sulphide and graphene nanocomposites as an anode for LIBs (see Table S1 in the Supporting Information).These results strongly indicate that PANI coating has important influence on enhancing the cyclic performance of the SnS_2 nanoplates, since PANI coating layers can buffer the volume expansion and contraction during the intercalation and de-intercalation process of Li ions. To prove this, we compared the SEM of the pristine SnS_2 and SnS_2@PANI nanoplates electrodes after 50 cycles of charge and discharge (see Figure S1 in the Supporting Information). As expected, the plate-like morphology of SnS_2@PANI nanoplates was basically retained after 50 cycles. In contrast, the pulverization of the pristine SnS_2 electrode was observed due to the aforementioned volume excursion effects.

Fig. 6d compares the rate performance of the pristine SnS_2 and SnS_2@PANI nanoplates electrodes at different current densities. With increasing the current density from 200 to 5000 mA g^{-1}, the discharge capacities of the two materials decrease, indicating the diffusion-controlled kinetics process for the electrode reaction. But it can clearly observed that the reversible capacity of SnS_2@PANI nanoplates was kept at 934.2 mAh g^{-1} after the 5th cycle at a current density of 100 mA g^{-1}. Upon increasing the discharge-charge rates to 200, 500, 1000 and 2000 mA g^{-1}, the reversible capacities were maintained at about 821.8, 726.8, 661.1 and 559.2 mAh g^{-1}, respectively. It was obviously that all the rate capacities of SnS_2@PANI nanoplates were higher than those of the pristine SnS_2. Even at a high current density of 5000 mA g^{-1}, the specific capacity remained at about 356.1 mAh g^{-1}, whereas that of the pristine SnS_2 dropped to only 147.6 mAh g^{-1}. When the current rate was again reduced back to100 mA g^{-1} after 30 cycles, the specific capacities of SnS_2@PANI nanoplates returned to about 800 mAh g^{-1}, which did not ultimately change in the subsequent cycles. Obviously, the result clearly demonstrates that the SnS_2@PANI nanoplates could tolerate varied discharge current densities and has a good application prospect in high power lithium-ion batteries. The excellent rate capability of the SnS_2@PANI nanoplates is probably rooted in its lamellar sandwich nanostructure. Conducting polymer PANI coating on the outer surface of the SnS_2@PANI nanoplates can provide a conductive network and buffer layer at high discharge rate.[29] What's more, the exfoliated SnS_2 nanoplates can shorten the transport lengths between SnS_2 nanoplates for both electrons

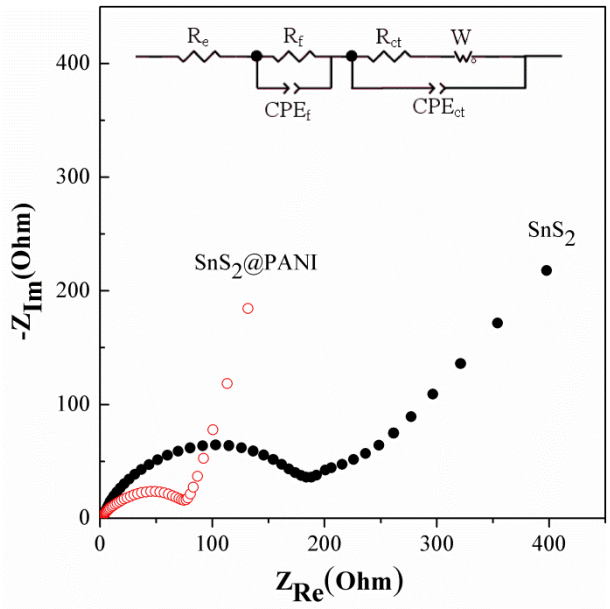

Fig. 7 Electrochemical impedance spectra of the SnS_2@PANI nanoplates and the pristine SnS_2 electrodes. The inset shows equivalent circuit model of the studied system.

and the lithium ions.

In order to understand the reasons for the improved high-rate performance, electrochemical impedance spectroscopy (EIS) measurements were carried out for the SnS_2@PANI nanoplates and the pristine SnS_2 electrodes after the 5th cycle at a current density of 100 mA g^{-1}, and the impedance plots of the two electrodes along with the equivalent circuit model are presented in Fig. 7. The Nyquist plots consisted of one depressed semicircle at high frequency and an inclined line at low frequency. Generally, the semicircle is associated with the internal resistance (R_e) of the battery, the resistance (R_f) and constant phase element (CPE_f) of SEI film, the charge transfer resistance (R_{ct}) and constant phase element (CPE_{ct}) of the electrode/electrolyte interface. The inclined line represents Warburg impedance (Z_w) related to the diffusion of lithium ions within the bulk of the electrode material. The SEI film resistance R_f and charge-transfer resistance R_{ct} of the SnS_2@PANI nanoplates electrode are 8.7 Ω and 65.32 Ω, which are much less than the corresponding value of the pristine SnS_2 electrode (13.16 Ω and 163.95 Ω). Obviously, the PANI coating can remarkably enhance the surface electronic conductivity of the materials and is propitious to fast transportation of electrons within the exfoliated SnS_2 nanoplates during electrochemical lithium insertion/extraction process, leading to significant improvement in the electrochemical performance of SnS_2@PANI nanoplates.

Based on above-mentioned experimental results, we believe that SnS_2@PANI nanoplates are a promising candidate as anode material of high-performance LIBs. The superior Li-battery performance of the SnS_2@PANI nanoplates electrode can be explained as follows: (i) the flexible lamellar sandwich structure in the obtained composite not only provide an elastic buffer layer to accommodate the volume expansion/contraction of SnS_2 during Li^+ insertion/extraction process,[29] but also efficiently prevent the restack of SnS_2 nanoplates and the crumbling of electrode material upon continuous cycling,[28] thus maintaining large capacity and high cycling stability. (ii) the well-connected PANI 2D networked structures in the composite can serve as the conductive channels between SnS_2 nanoplates, which decreases the inner resistance of LIBs, therefore leading to a higher specific capacity.[28] (iii) Li-ion diffusion strongly depends on the transport length.[38] The exfoliated SnS_2 nanoplates in the nanocomposite offer improved energy storage capacity, coulombic efficiency, and better cycling stability due to short path length for Li^+ transport and good stability for nanostructured electrodes.

4. Conclusions

The novel anode material in the form of a SnS_2@PANI nanoplates was synthesized by in situ oxidative polymerization of aniline on the surface of ultrasonic exfoliated SnS_2 nanoplates. The as-obtained nanocomposite presents a flexible lamellar sandwich structure and good electrical conductivity. As a result, SnS_2@PANI nanoplates shown high reversible capacity (730.8 mAh g^{-1} after 80 cycles) and excellent rate capability (356.1 mAh g^{-1} at the rate of 5000 mA g^{-1}) The impressive electrochemical performance may be attributed to the synergic effect of lamellar structured SnS_2 and conducting polymer PANI. Our study not only provides a simple and efficient synthesis strategy for various inorganic–organic nanocomposites obtained by exfoliation of layered inorganic materials, but also helps in designing novel and high performance electrode materials.

Acknowledgements

We would like to thank Prof. Jianyi Lin (Institute of Chemical and Engineering Sciences (ICES), Agency for Science, Technology and Research (A*STAR)) for his helpful discussions. This work was financially supported by Program for Changjiang Scholars and Innovative Research Team in University (PCSIRT, No. IRT1161), Program of Science and Technology Innovation Team in Bingtuan (No 2011CC001), and the National Natural Science Foundation of China (No. 21263021,U1303291).

Notes and references

1 B. Dunn, H. Kamath and J. Tarascon, Science, 2011,334, 928.
2 J.B. Goodenough, Accounts of Chemical Research, 2013,46, 1053.
3 J. W. Seo, J. T. Jang, S. W. Park, C. J. Kim, B. W. Park and J. W. Cheon, Adv. Mater., 2008, 20, 4269.
4 L. Mei, C. Xu, T. Yang, J. Ma, L. Chen, Q. Li and T. Wang, J. Mater. Chem. A, 2013, 1, 8658.
5 C. X. Zhai, N. Du, H. Zhang and D. R. Yang, Chem. Commun., 2011, 47, 1270
6 H. Mukaibo, A. Yoshizawa, T. Momma and T. Osak, J. Power Sources, 2003, 119-121, 60.
7 H. S. Kim, Y. H. Chung, S. H. Kang and Y. E. Sung, Electrochim. Acta, 2009, 54, 3606.
8 C. X. Zhai, N. Du, H. Zhang, J. X. Yu and D. R. Yang, ACS Appl. Mater. Interfaces, 2011, 3, 4067.
9 K. Chang, Z. Wang, G. Huang, H. Li , W. Chen, J. Y. Lee, J. Power Sources, 2012, 201, 259.
10 Q. Zhang, R. Li, M. Zhang, B. Zhang and X. Gou, Electrochim. Acta, 2014, 115, 425.
11 X. Jiang, X. Yang, Y. Zhu, J. Shen, K. Fan and C. Li, J. Power Sources, 2013, 237, 178.
12 Z. F. Jiang, C. Wang, G. H. Du, Y. J. Zhong and J. Z. Jiang, J. Mater. Chem., 2012, 22, 9494.
13 B. Luo, Y. Fang, B. Wang, J. S. Zhou, H. H. Song and L. J. Zhi, Energy Envir. Sci., 2012, 5, 5226.

14 S. Liu, X. Lu, J. Xie, G. Cao, T. Zhu and X. Zhao, ACS Appl. Mater. Interfaces, 2013, 5, 1588.
15 D. Kong, H. He, Q. Song, B. Wang, Q.-H. Yang and L. Zhi, RSC Adv., 2014, 4, 23372.
16 M. Zhang, D. Lei, X. Yu, L. Chen, Q. Li, Y. Wang, T. Wang and G. Cao, J. Mater. Chem., 2012, 22, 23091.
17 J. Yin, H. Cao, Z. Zhou, J. Zhang and M. Qu, J. Mater. Chem., 2012, 22, 23963.
18 L. Zhuo, Y. Wu, L. Wang, Y. Yu, X. Zhang and F. Zhao, RSC Adv., 2012, 2, 5084.
19 Q. Wu, L. Jiao, J. Du, J. Yang, L. Guo, Y. Liu, Y. Wang and H. Yuan, J. Power Sources, 2013, 239, 89.
20 J. Ma, D. Lei, X. Duan, Q. Li, T. Wang, A. Cao, Y. Mao and W. Zheng, RSC Adv., 2012, 2, 3615.
21 J. T. Zai, K. X. Wang, Y. Z. Su, X. F. Qian and J. S. Chen, J. Power Sources, 2011, 196, 3650.
22 L. Wang, L. Zhuo, Y. Yu and F. Zhao, Electrochim.Acta, 2013, 112, 439.
23 T. J. Kim, C. Kirn, D. Son, M. Choi and B. Park, J. Power Sources, 2007, 167, 529.
24 C. X. Zhai, N. Du, H. Zhang and D. R. Yang, Chem. Commun., 2011, 47, 1270.
25 Q. Wu, Y. Xu, Z. Yao, A. Liu, and G. Shi, ACS Nano, 2010, 4, 1963.
26 X. Zhang, L. Jia, S. Zhang and W. Yang, J. Power Sources, 2007, 173, 1017.
27 T. A. Kerr, H. Wu and L. F. Nazar, Chem. Mater., 1996, 8, 2005.
28 L. Zheng, Y. Xu, D. Jin and Y. Xie, Chem. Asian J., 2011, 6, 1505.
29 Y.-G. Wang, W. Wu, L. Cheng, P. He, C.-X. Wang and Y.-Y. Xia, Adv. Mater., 2008, 20, 2166.
30 S. Ghosh and O. Inganas, Adv. Mater., 1999, 11, 1214.
31 S. Wang, Q. Gao, Y. Zhang, J. Gao, X. Sun and Y. Tang, Chem. Eur. J., 2011, 17, 1465.
32 J. Morales, C. Perez-Vicente and J. L. Tirado, Solid State Ionics, 1992, 51, 133.
33 Y. P. Du, Z. Y. Yin, X. H. Rui, Z. Y. Zeng, X. J. Wu, J. Q. Liu, Y. Y. Zhu, J. X. Zhu, X. Huang, Q. Y. Yan and H. Zhang, Nanoscale, 2013, 5, 1456.
34 M. Sathish, S. Mitani, T. Tomai and I. Honma, J. Phys. Chem. C, 2012, 116, 12475.
35 S. Ding, J. S. Chen, G. Qi, X. Duan, Z. Wang, E. P. Giannelis, L. A. Archer and X. W. Lou, J. Am. Chem. Soc, 2011, 113, 21.
36 D. Aurbach, A. Nimberger, B. Markovsky, E. Levi, E. Sominski and A. Gedanken, Chem. Mater., 2002, 14, 4155.
37 C. Liu, F. Li, L.-P. Ma, H.-M. Cheng, Adv. Mater., 2010, 22, E28.
38 Y. G. Guo, J. S. Hu and L. J. Wan, Adv. Mater., 2008, 20, 2878.